Published in final edited form as:
*Int J Cancer*. 2011 May 15; 128(10): 2481–2494. doi:10.1002/ijc.25587.

# A water soluble parthenolide analogue suppresses *in vivo* tumor growth of two tobacco associated cancers, lung and bladder cancer, by targeting NF-κB and generating reactive oxygen species

**Rajasubramaniam Shanmugam**[1], **Praveen Kusumanchi**[1], **Hitesh Appaiah**[2], **Liang Cheng**[3], **Peter Crooks**[4], **Sundar Neelakantan**[4], **Tyler Peat**[5], **James Klaunig**[5], **William Matthews**[6], **Harikrishna Nakshatri**[2,7,8], and **Christopher J Sweeney**[1,9]

[1]Department of Medicine, Indiana University, Indianapolis, IN, USA

[2]Department of Surgery, Indiana University, Indianapolis, IN, USA

[3]Department of Pathology, Indiana University, Indianapolis, IN, USA

[4]College of Pharmacy, University of Kentucky, Lexington, KY, United States

[5]Department of Pharmacology and Toxicology, Indiana University, Indianapolis, IN, USA

[6]Leuchemix Inc, Woodside, California, USA

[7]Walther Cancer Institute, Indianapolis, IN, USA

[8]Department of Biochemistry and Molecular Biology, Indiana University, Indianapolis, IN, USA

[9]Department of Medical Oncology, Dana Farber Cancer Institute, Boston, MA, USA

## Abstract

Dimethylaminoparthenolide (DMAPT) is a water soluble parthenolide analogue with preclinical activity in hematologic malignancies. Using NSCLC cell lines (A549, H522) and an immortalized human bronchial epithelial cell line (BEAS2B) and TCC cell lines (UMUC-3, HT-1197, HT-1376) and a bladder papilloma (RT-4), we aimed to characterize DMAPT's anti-cancer activity in tobacco associated neoplasms. Flow cytometric, electrophorectic mobility gel shift assays (EMSA), and western blot studies measured generation of reactive oxygen species (ROS), inhibition of NFκB DNA binding, and changes in cell cycle distribution and apoptotic proteins. DMAPT generated ROS with subsequent JNK activation and also decreased NFκB DNA binding and anti-apoptotic proteins, TRAF-2 and XIAP. DMAPT induced apoptotic cell death and altered cell cycle distribution with upregulation of p21 and p73 levels in a cell type dependent manner. DMAPT suppressed cyclin D1 in BEAS2B. DMAPT retained NFκB and cell cycle inhibitory activity in the presence of the tobacco carcinogen nitrosamine ketone, 4(methylnitrosamino)-1-(3–pyridyl)-1-butanone (NNK). Using a BrdU accumulation assay, 5 to 20μM of DMAPT was shown to inhibit cellular proliferation of all cell lines by more than 95%. Oral dosing of DMAPT suppressed *in vivo* A549 and UMUC-3 subcutaneous xenograft growth by 54% (p=0.015) and 63% (p<0.01) respectively and A549 lung metastatic volume by 28% (p=0.043). In total this data demonstrates DMAPT's novel anti-cancer properties in both early and late stage tobacco

[*]**Corresponding Author:** Christopher J Sweeney, MBBS; Dana Farber Cancer Institute, 44 Binney Street, DA-1230, Boston, MA, 02115, USA ; Phone: +1 617 632 4534 ; Fax:+1 617 632 2165; christopher_sweeney@dfci.harvard.edu.

CJS, HN, PC and WM are founders of and hold stock in the company, Leuchemix, which is developing dimethylaminoparthenolide (DMAPT).

associated neoplasms as well as its significant *in vivo* activity. The data provides support for the conduct of clinical trials in TCC and NSCLC.

**Keywords**

Dimethylaminoparthenolide; cell cycle; apoptosis; cancer

## INTRODUCTION

In the USA in 2008, over 68,000 individuals were diagnosed with bladder cancer, and more than 14,000 patients died from their disease. Transitional cell carcinoma (TCC) is the dominant histology in over 95% of cases1. There were also more than 200,000 patients diagnosed with lung cancer with 160,390 deaths and non-small lung cancer makes up more than three quarters of these cases1. Tobacco smoking is a major modifiable risk factor for both bladder and non-small lung cancers (NSCLC) and significant achievements in decreasing this risk factor have been made in some countries. Despite this progress, these cancers are still a major cause of the current death rate from cancer2. Modest advances have recently been made in the treatment of NSCLC with epidermal growth factor receptor and angiogenesis inhibition3, 4. Therefore, novel strategies are needed to prevent the progression of epithelial cells which have entered the neoplastic process, prevent emergence of micrometastatic lesions after resection and treat established cancers.

Parthenolide, a sesquiterpene lactone obtained from the plant *Tanacetum parthenium*, concurrently promotes apoptosis in neoplastic cells by inducing oxidative stress while inhibiting the cancer promoting transcription factor, nuclear factor kappa B (NFκB). These unique properties are due to its α-methylene-γ-lactone ring and epoxide interacting with nucleophilic sites of biological molecules5 which in turn generates ROS by depleting glutathione and other thiols and activates caspases and apoptosis6. Parthenolide decreases NFκB DNA binding by both inhibiting IκB kinase and by directly preventing the p65 protein binding to DNA5, 7. Inhibition of NFκB signaling leads to reduced expression of many proteins including anti-apoptotic proteins including Tumor necrosis factor receptor-associated factor (TRAF)-1 and TRAF-28. The downstream consequences of these effects include activation of p53 and caspases with consequent cell cycle arrest and promotion of cell death6, 9, 10.

However, parthenolide has poor pharmaceutical properties and cannot be detected in plasma when humans have been given it as part of the herbal supplement, "*feverfew*"11. We have also shown it has limited *in vivo* activity due to the poor bioavailability12. Hence, the aminoanalogue, dimethylaminoparthenolide (DMAPT) was developed13 and entered phase 1 clinical trials after documenting 70% oral biovailability, plasma concentrations in excess of 40μM after oral administration and an acceptable toxicology profile in animal studies (unpublished data).

In this paper we describe the *in vitro* and *in vivo* activity of DMAPT in two smoking related cancers, lung and bladder cancer as well as its ability to generate ROS, inhibit NFκB and both promote apoptosis and induce cell cycle arrest in a cell type dependent manner. These findings are detailed for both early and late stage NSCLC and TCC, and are shown to be both independent of p53 status and retained in the presence of the tobacco carcinogen, NNK. In so doing, this work adds to the data supporting the conduct of DMAPT clinical trials in hematological and solid tumor malignancies14-19.

## MATERIALS AND METHODS

### Cell culture and treatment

DMAPT powder was produced13 from parthenolide sourced from Biomol (Pennsylvania, USA) and dissolved in sterile water. All cell lines were purchased from American Type Culture Collection (Manassas, VA) and kept in culture per specifications. Lung cancer cell lines: A549 (wild type (wt) p53 20; wt retinoblastoma (Rb) 21]; H522, (mutant p53 22; wt Rb 23), and BEAS2B (wt p53 24 wt Rb25 but immortalized with SV40 large T antigen effecting RB and p53 function26, 27). Bladder cell lines were: UMUC-3 (mutant p53, wt Rb28); HT1197 (mutant p53, mutant Rb28); HT1376 (mutant p53, mutant Rb28); and RT4 (wild type p53, mutant Rb28). NNK was purchased from Toronto Research Chemicals (ON, Canada) and dissolved in water and added to the assays at the indicated time-points.

### Western Blotting

Cell lines were treated with varying concentrations of DMAPT and after indicated durations, the medium was removed and the attached cells were washed with PBS. Whole cell proteins were extracted in protein extraction buffer (50mM Tris pH 7.5, 0.25% sodium deoxycholate, 1% NP40, 150mM NaCl, 1mM EDTA, 100μM sodium orthovandate, 1mM sodium fluoride, 1mM β-glycerophosphate, 0.5mM PMSF, 2μg/ml aprotenin, leupeptin and pepstatin). Protein concentrations were measured with Bio-Rad Protein assay reagent (Bio-Rad Laboratories Inc. Hercules, CA). Equal amounts of total protein (50μg) were loaded and run on 10% SDS-polyacrylamide gel with Trisglycine running buffer and then transferred to a nitro-cellulose filter. The filters were blocked with Tris-buffered saline containing 5% non-fat milk at 4°C overnight then probed. Antibodies against phosphoJNK, phospho-cJun, cJun, JNK, GAPDH were procured from Cell Signaling (Beverely, MA), p21, p65, from Santa Cruz Biotechnology (Santa Cruz, CA) and TRAF2, XIAP, Caspase 8 from B.D. Biosciences (San Diego CA). Experiments were repeated 2-4 times with similar results.

### Electrophoretic mobility Gel Shift Assay (EMSA)

All cell lines tested were harvested in exponential growth phase. DMAPT was added three hours prior to harvesting whole cell protein. EMSA was carried out as described earlier8. To evaluate the effect of N-acetyl cysteine (NAC) on NFκB DNA binding, cells were exposed to NAC for 1 hour before DMAPT treatment. DNA binding activity of Oct 1 was measured as a control in untreated and DMAPT treated cellular extracts. DNA-protein complexes were separated by electrophoresis and visualized by autoradiography.

### Determination of cellular ROS

ROS production was detected using 2',7'-dichlorodihydroflourescein diacetate ($H_2$DCFDA), a cell-permeable fluorescent probe (Invitrogen-Molecular Probes, Carlsbad, CA). Exponentially growing cells were loaded with 10μmol/L $H_2$DCFDA for 45 minutes before treatment at 37° C and were washed with PBS. The cells were allowed to recover for 15 minutes at 37°C in growth media and then treated with DMAPT alone or in presence of NAC. Following treatment, cells were washed in PBS and the green fluorescence intensity in cells was examined by FACS analysis.

### Apoptosis analysis

For measurement of apoptosis, Annexin V assay (Vybrant Apoptosis Kit # 3; Invitrogen, Carlsbad, California) was performed according to the manufacturer's instructions. Briefly, floating and adherent cells were harvested after exposure to DMAPT for 24 and 36 hours, washed twice with PBS, incubated with FITC-conjugated Annexin V and Propidium Iodine

(PI) for 15 minutes, and analyzed by FACScan (Becton Dickinson Bedford, MA). Experiments were performed with and without NAC pretreatment.

### Cell cycle analysis

Cell cycle analysis by flow cytometry was undertaken of adherent cells only ($2 \times 10^5$). The cells had been plated on a 60-mm plate, harvested by trypsinization then pelleted, and re-suspended in 1 mL of PBS. After spinning, cells were re-suspended in 125μl of PBS with 2mg/ml RNase A. Cells were further stained with 50 μg/mL propidium iodide (PI) solution (300 μl). Cell cycle analysis was carried out with a Becton Dickinson (Bedford, MA) FACScan flow cytometer. Data were analyzed with the Modfit LT software (Verity Software House, Inc., Topsham, ME).

### RNA isolation and Reverse Transcription-Polymerase Chain Reaction (RT-PCR)

Total RNA was extracted from the cell lines using RNeasy kit (Qiagen, MD) according to manufacturer's instructions. Total RNA (1ug) was then reverse transcribed using the Superscript First Strand- synthesis kit (Invitrogen Life Technologies, Inc.). Five percent of the cDNA was used for each gene specific PCR. The reaction cycle was started by denaturation at 95°C for 5 min, followed by TAp73 specific condition 40 cycles at 94°C (30 s), 56°C (40 s), and 72°C (30 s) using (sense, 5'-TCTCTGGAACCAGACAGCAC-3') and (antisense, 5'-GGGGTAGTCGGTGTTGGAG-3'). P21 was amplified using p21 specific primers (sense 5' GCGACTGTGATGGCGTAATG-3') and (anti-sense) 5'AGAAGATCAGCCGGCGTTTG-3') with 30 cycles 94°C (30 seconds), 60°C (45 seconds) and 72°C (45 seconds). The Actin gene was chosen as an endogenous expression control (Sense 5'-GCACCACACCTTCTACAATGAGC-3') and (anti-sense '-GGATAGCACAGCCTGGATAGCAAC-3') with 30 cycles 94°C (1min), 55°C (1min), and 72°C (1min). Fifteen μl of RT-PCR products were resolved in 2.0% agarose gels and were imaged and quantified with LabWorks analysis software (UVP Products, Cambridge, United Kingdom).

### Small interfering RNA (siRNA) treatment

siRNA for luciferase (non-specific siRNA control) p53 and p73 and the siRNA non-target control were purchased from Dharmacon RNAi Technologies (Lafayette, Colorado, USA). The UMUC-3 cells ($4\times10^4$) were seeded into a 6-well dish and left for 24 hours. On the following day a 2.5 μL aliquot of siRNA solution (20pmol/μL) and 175 μl of Opti-MEM (Invitrogen) and 16μL Opti-MEM + 3μL of Oligofectamine (Invitrogen) were each mixed separately. They were incubated for 20 min at room temperature after combining the two mixtures, and then added to the cells which had been seeded on the dish. The siRNA-transfected cells were used after 96 hours.

### Proliferation assays

Cellular proliferation was measured using the Cell Proliferation ELISA, BrdU Kit (Roche, Indianapolis,IN) according to manufacturer's instructions. Cell lines were plated in a 96-well plate in 100 μL of media and incubated in 5% $CO_2$ at 37°C for 24h. After 24 hours of plating, varying concentrations of DMAPT in 5 μl of media were added to each well and amount of cellular proliferation relative to untreated control was determined 48 hours after addition of DMAPT.

### Trypan Blue exclusion test for cell viability

0.5 million cells were placed in a 100mm plate and drugs added at 24 hours when in exponential growth phase. Cells were harvested at 48 hours after drug exposure by trypsinization, made into a pellet and resuspended in PBS. Cells were diluted 1:1 ratio with

Trypan Blue (0.4%, Sigma) and placed in a hemacytometer and counted for viable (opaque) and non-viable cells (stained blue).

### In Vivo Tumor Model

Male nude athymic mice aged 6–8 weeks were procured (Harlan Sprague Dawley Bioproducts for Science, Indianapolis, IN) and acclimatized for 1 week. A549 and UMUC-3 cells suspended in Matrigel (12-18mg/ml) (Trevigen; Gaithersburg, MD) at a concentration of $1\times10^6$ cells per mL were injected into the subcutaneous tissue of the flank. The tumors were allowed to establish for 7 days prior to drug treatment and the mice were sorted with 10 mice per cohort for UMUC-3 and A549. Animals received either solvent control daily or the indicated doses of DMAPT either daily or twice daily by oral gavage. The mice were maintained in a pathogen-free environment with free access to food and water. Body weight and tumor volume (using formula [sagittal dimension (mm) × cross dimension2 (mm)] ÷ 2 were measured twice weekly. Unpaired t tests were used to statistically compare the final tumor volumes. In the lung metastasis model, one million cells were injected into the tail vein of female athymic nude mice and DMAPT treatment commenced the following day and treated daily for 60 days29. The mice were sacrificed and lungs removed and fixed in formalin and embedded in paraffin and stained with hematoxylin and eosin (H&E). The relative volume of lung metastasis was calculated by a technician blinded to treatment arm and using lung tissue stained with H&E. Normal tissue and adenocarcinoma areas were evaluated using a Bioquant Image Analyzing System (Version 1769, Bioquant Image Analysis Corp.; Nashville, TN). Stereological methods were used to calculate the relative volume of adenocarcinoma per lung30. The sum of all adenocarcinomas per slide was divided by 1,000,000 for a total area in $mm^2$; this value was divided by the total area (in $mm^2$) of all lung tissue for each particular mouse and multiplied by 100 to obtain the relative volume (in $mm^3$).

### Immunohistochemistry

Immunohistochemical studies were performed on paraffin-embedded tissue sections. Serial sections (5-mm thick) of paraffin-embedded tissues were fixed on silane coated glass slides, deparaffinized, and rehydrated in tap water. Antibodies used were TRAF2 (clone 33A1293; Abcam, Cambridge, UK) at dilution 1:200, and p21 (Calbiochem, Cat. OP64F) at 1:200. Antigen was retrieved using Target retrieval system (TRS, DAKO S1700) for 20 minutes at 95°C. Sections were blocked with Avidin-Biotin blocking system (DAKO) for 10 minutes and the endogenous peroxidase was quenched with 3%$H_2O_2$ for 15 minutes. Background was blocked using DAKO protein block for 30 minutes followed by primary antibody for 1 hr (2 mg/ml). Sections were exposed to secondary donkey anti-body (30 min) and horseradish peroxidase- linked DAKO streptavidin for 30 minutes in 3,30-diaminobenylin tetrahydrocholoride(DAB) as chromogen and counterstained with hematoxylin. The extent and intensity of staining in the cancer cells were evaluated by a single investigator blinded to the treatment arm. Microscopic fields were evaluated and those with the highest degree of immunoreactivity were pictured.

## RESULTS

### DMAPT generates reactive oxygen species (ROS) in both TCC and NSCLC cell lines with associated activation of JNK pathway

We confirmed the ability of DMAPT (10μM) to induce ROS6, 31 in lung and urothelial neoplastic cell lines as measured by FACS (Figure 1A) in UMUC-3 (upper panel) and A549 (lower panel). ROS generation was also observed in RT4 (data not shown) but to a lesser degree than the more advanced cancerous cell lines. The growth media of BEAS2B (BEGM, Lonza, Walkersville) contained Phenol red and interfered with the FACS. Pre-treatment with

the anti-oxidant N-Acetyl Cysteine (NAC) blocked ROS generation in all cell lines due to its ability to elevate intracellular cysteine. This provides an abundance of intracellular glutathione to prevent the generation of ROS. It is of note that parthenolide activity is also blocked by other general antioxidants such as pyrrolidine dithiocarbamate (0.25μM), and nordihydroguaiaretic acid (0.1 μM), and that inhibition of glutathione synthesis with buthionine sulfoximine, sensitizes the cells to parthenolide6, 31. Moreover, 0.5 to 1mM of NAC is required to block DMAPT. This is 100 times in excess of the DMAPT concentration and one would expect DMAPT blockade at lower NAC doses if it was due to a direct interaction between DMAPT and NAC rather than the latter being a source of glutathione.

Activation of c-Jun N-terminal kinase (JNK) is one of the best studied downstream effects of ROS generation32 and DMAPT's ability to generate ROS was associated with phosphorylation of c-JUN in A549, H522 and UMUC-3 cells and increased total JNK and phosphorylation of JNK in UMUC3 (Supplementary Figure 1). This was blocked by NAC (Figure 1B)

## DMAPT inhibits NFκB DNA binding and decreases proteins under its control in both urothelial and lung neoplastic cell lines

EMSA confirmed the presence of constitutive NFκB DNA binding in the cell lines and DMAPT's ability to inhibit NFκB DNA binding (cells exposed to DMAPT for 3 hours) in both the advanced (UMUC-3 and A549) and early (RT4 and BEAS2B) neoplastic cell lines (Figures 1C and D). The inhibition was dose dependent with 10 to 20μM causing a marked decrease in the cell lines tested. A kinetic analysis of NFκB DNA binding with time points of 0.5, 1, 2.0 and 3.0 hours (Supplementary Figure 3) showed the decrease in NFκB DNA binding begins at 1 hour and is more pronounced at 2 and 3 hours. Proteins regulated by NFκB were decreased by DMAPT in a time, dose and cell dependent manner (Figures 1E). The effective DMAPT doses were in the low micromolar range and corresponded with the doses which partially or completely inhibited NFκB DNA binding. It is of note a longer exposure (24 hours) to a lower dose (5μM DMAPT) was more effective than 10μM for 12 hours in decreasing TRAF-2 in UMUC-3 (left panel). In RT4 10μM DMAPT was effective at 12 hours but not at 24 hours in decreasing XIAP (right panel). DMAPT (20μM) also decreased NFκB regulated proteins of TRAF-2 in A549 from 6 to 24 hours (right panel) but no change was seen in TRAF-2 or XIAP in BEAS2B (data not shown). In total the data indicates the dose, time and ability of DMAPT to decrease NFκB regulated proteins is cell dependent and does not always correspond to the amount of inhibition of NFκB DNA binding at 3 hours.

## DMAPT inhibits proliferation and decreases the viability of early and late lung and urothelial cell lines in a dose dependent manner

In general, the doses that caused the inhibition of proliferation, when measured using a BrdU accumulation assay, by greater than 95% (10 and 20μM) corresponded with the doses that blocked NFκB DNA binding in UMUC-3 and A549 cells (Figure 2A). This was also observed in HT1376 and HT1197 (EMSA data not shown). In contrast, the earlier neoplastic lesions RT4 (papilloma) and BEAS2B (immortalized human bronchial epithelial cell line) had greater than 80% inhibition of proliferation with 5μM but required 3 hours of DMAPT exposure at 10μM (BEAS2B) or 20μM (RT4) before substantially inhibiting NFκB DNA binding. The trypan blue assay showed that after one dose the viability for each cell line at 48 hours was 26.2% for A549 with 20μM, 20.9% for BEAS2B with 5μM; 11.8% for UMUC-3 with 10μM and 13.4% for RT4 with 10 μM. Also in A549 cells with intact and siRNA p53 or p73 we were able to observe DMAPT's ability to inhibit proliferation when p53 or p73 were reduced (Supplementary Figure 2).

NAC abrogated DMAPT's ability to suppress proliferation of UMUC-3, A549 and BEAS2B in a dose dependent manner(Figure 1B). Given this observation we then sought to discern whether NACs' effect was purely by blocking the oxidative stress and independent of DMAPT's ability to block NFκB DNA binding. Using the EMSA for NFκB DNA binding in UMUC-3 cells, it was noted that NAC blocked DMAPT's ability to inhibit NFκB DNA binding in a dose dependent manner. (Figure 2B, bottom right panel). These results suggest that DMAPT generation of ROS may be the initiating event and the subsequent reactions impact the NFκB DNA binding.

### DMAPT causes alteration of cell cycle in a cell type dependent manner

Because parthenolide alters the cell cycle by a number of possible mechanisms an evaluation of DMAPT's ability to alter effectors of cell cycle (p73 and p21) was undertaken in advanced cancer cell lines with both functional p53 (A549) and mutant p53, (UMUC-3). In both cell lines DMAPT was able to increase p73 as measured by PCR (Figure 3A, left panel and C, left panel) as well as p21 (Figure 3B and C, right panel). Both siRNA inhibition of p73 and NAC exposure only partially blocked DMAPT's ability to increase p21 expression in UMUC-3 (Figure 3B). It is of note that the time course studies in A549 (Figure 3C) of p21 and p73 transcription showed that DMAPT mediated p21 increase occurred prior to the p73 increase and was at the time DMAPT started to decrease NFκB DNA binding at one hour (Supplementary Figure 3). Altogether, this data indicates p73 has, at most, only a partial role in inducing p21 expression in UMUC-3 and appears not to be related to p21 induction in A549. The time course studies showing that the beginning of DMAPT mediated inhibition of NFκB DNA binding (i.e one hour) coincides with the p21 increase suggests a possible relationship between these two events in A549 cells.

FACS demonstrated DMAPT induced accumulation of cells in S phase at 12 and 24 hours in UMUC-3 (p53 mutant, functional Rb) with 10μM (Figure 4D, top panel) and that this was blocked by NAC. In contrast, A549 cells with wild type p53 and functional Rb undergo transient G2 accumulation upon treatment with 20μM DMAPT (Figure 4D, bottom panel). Specifically, NAC sensitive G2 accumulation was evident at 12 hours but not 24 hours after treatment. It is interesting to note that 20 μM of DMAPT was required for the cell cycle effects on A549 cells, which is consistent with less sensitivity of these cells to DMAPT in cell proliferation assays (Figure 2D).

### DMAPT induces apoptosis

In prior work, parthenolide has been shown to induce apoptosis as measured by flow cytometry with propidium iodine and Annexin V staining33. This was also confirmed with 10μM DMAPT in both early and late stage TCC and NSCLC [UMUC-3, RT 4, BEAS2B and A549] (Figures 4 A, C, D, E). A549 cells treated with 10 μM DMAPT had a less robust increase of cells undergoing apoptosis at this concentration, consistent with the results of cell proliferation and cell cycle analysis, where 20 μM was more effective. In all cell lines that underwent apoptosis, the type of apoptosis observed was both early and late apoptosis. In BEAS2B, necrosis was also evident. All types of DMAPT induced cell death were inhibited by NAC. We further characterized apoptotic events in UMUC-3 cells. DMAPT decreased the levels of procaspase 8 and procaspase 3 and induced the apoptosis-specific cleavage of PARP in a time and dose dependent manner (Figure 4B). We were not able to detect active caspase 8 or 3 in these cells (presumably due to labile nature of active caspases).

### DMAPT blocks NNK-induced activation of NFκB and retains cell cycle inhibitory activity in the presence of NNK

To explore the ability of DMAPT to negate molecular biological events that drive aberrant cellular proliferation of cells earlier in the neoplastic process, a urinary bladder papilloma (RT4) and an immortalized human bronchial epithelial cell line (BEAS2B) were studied. Both cell lines displayed modest levels of NFκB DNA binding activity (Figure 5A and B right panel). The tobacco carcinogen, NNK, increased NFκB DNA binding in BEAS2B in a dose dependent manner but did not alter it in RT4. DMAPT efficiently reduced NFκB activation in both cell lines and this was not abrogated when NNK was given after DMAPT (5A right panel and 5B right panel). The NNK induced increase in NFκB DNA binding in BEAS2B cells was associated with an increase in cyclin D1 and this was blocked when the cells were pretreated with DMAPT. Neither NNK alone nor DMAPT alone altered cyclin D1 expression in RT4 cells (data not shown) indicating the cell type dependent effects from NNK exposure.

FACS evaluated whether DMAPT impacted the cell cycle in these “early” neoplastic cells either when given alone or in the presence of NAC. There were cell type specific differences in cell cycle stages. DMAPT treatment of RT4 cells lead to an accumulation in S phase (Figure 5C, top panel), similar to the other bladder cancer cell line UMUC-3. In contrast, DMAPT treatment of BEAS2B, accumulated cells in G2 phase at both 12 and 24 hours after exposure (Figure 5C, bottom panel). This was similar but more durable to the findings in the lung cancer cell line A549. These changes were blocked by NAC in both cell lines.

We next examined the effect of DMAPT on cell cycle under NNK exposure (Figure 5D). NNK alone did not alter cell cycle distribution in RT4 (top panel). DMAPT in the presence of NNK maintained the ability to increase the number of RT4 cells in S phase. This suggests that DMAPT retains its ability to function in RT4 cells in the presence of tobacco carcinogens. In contrast, NNK alone did have an effect in BEAS2B and increased the percentage of cells in G1 phase in BEAS2B. DMAPT treatment followed by NNK increased the number of cells in G1 and S phases with a proportional decrease in G2 phase cells (unlike that seen with DMAPT alone in BEAS2B). These NNK specific effects in BEAS2B are consistent with NNK-induced cyclin D1 expression in this cell line. Specifically, cyclin D1 promotes the progression of the cell cycle from G1 to S phase. It is therefore consistent that DMAPT prior to NNK, by preventing an increase of cyclin D1, slowed progression of cells cycling from G1/S to G2 with a decrease of cells reaching the G2 phase (as was seen in Figure 5D, bottom panel).

### DMAPT's single agent *in vivo* anti-cancer activity in non-small cell lung and transitional cancer cell lines is associated with upregulation of p21 and decreased TRAF-2 expression

The single agent *in vivo* anticancer activity of DMAPT was confirmed using subcutaneous xenografts of UMUC-3 and A549 in athymic nude mice. Daily oral DMAPT treatment slowed the growth of both A549 and UMUC-3 cell lines (Figure 6A). At day 65, 100 mg/kg/day of oral DMAPT suppressed A549 subcutaneous xenograft tumor growth by 54% versus control ($p=0.016$). In UMUC-3 there was a dose dependent effect and 100 mg/kg oral twice per day suppressed tumor growth by 63% ($<0.001$). A lung metastasis model showed the ability of single agent DMAPT to decrease the metastatic burden of NSCLC cells (A549 cells injected via tail vein) in nude mice (Figure 6A, right panel). With 40 mg/kg/day of DMAPT, 29% of the lung volume was replaced with cancer versus 39% with the solvent control ($p=0.043$). As depicted by immunohistochemical staining of tumors at the time of sacrifice of both A549 and UMUC-3 subcutaneous xenograft experiments, DMAPT was able to upregulate p21 nuclear expression while decreasing TRAF-2 expression in both cell

lines (Figure 6B and C). This provided *in vivo* correlation of the *in vitro* findings of DMAPT treatment in these cell lines.

## DISCUSSION

The data presented details the anti-proliferative activity of DMAPT, a bioavailable analogue of parthenolide, in both early and late stage neoplastic lung and urothelial cells. Its activity is independent of p53. Moreover, single agent DMAPT is able to significantly decrease *in vivo* growth in both subcutaneous xenograft models tested as well as decrease the burden of metastatic disease from circulating tumor cells. The latter is presumably due to reducing circulating tumor cell implantation (one of the early phases of metastatic development)29 based on the fact therapy was started day 1 after tail vein injection. It is of note that the mice tolerated the therapy well. This preferential anti-cancer activity on neoplastic cells may be due to their dependence on NFκB14 and/or cancer cells having less capacity for dealing with ROS (eg less GSTπ in cancer cells to generate glutathione)6, 31. The ongoing phase 1 trial will determine the therapeutic window in humans.

The process by which DMAPT inhibits cancer cell proliferation is complex and cell type dependent. In this context, DMAPT resembles other natural compounds such as Curcumin34. However, DMAPT's good oral bioavailability and single agent *in vivo* activity is a distinguishing feature and is permitting clinical evaluation of DMAPT. The data presented indicates DMAPT both promotes apoptosis and slows progression through the cell cycle in a cell type dependent manner. These changes occurred at a dose level (5 to 20μM) achievable in the plasma after oral gavage. It is also proposed that the myriad of DMAPT effects seen at the 5 to 20μM exposure level are not “off target” effects but downstream effects from the chemical reaction of DMAPT's α-methylene-γ-lactone ring and epoxide interacting with nucleophilic sites of biological molecules5. This notion is supported by the fact the activity is consistently between 5 to 20μM and this dose range is associated with inhibition of NFκB DNA binding and proteins under its control. DMAPT's complex and multiple effects probably account for its broad activity in multiple cell types. This is in contrast to drugs with a specific target and a well defined patient population (such as traztuzumab which is active only in HER-2 overexpressing cancers35). The following discussion summarizes the molecular events that are thought to explain these complex and cell type dependent events.

The oxidative stress from ROS generation and NFκB activation are inter-related. NFκB can be activated by oxidative stress which can protect the cells from JNK mediated apoptosis.36 However, previous work with parthenolide and DMAPT has shown that these agents induce oxidative stress as an early event and then inhibit NFκB14. It is also known that NFκB DNA binding is redox sensitive37. It is therefore proposed that DMAPT inhibition of NFκB DNA binding is due to a combination of DMAPT's alteration of redox state from ROS generation combined with a direct effect on NFκB DNA binding. The ability of NAC to overcome DMAPT-mediated inhibition of NFκB DNA binding supports at least some relationship with ROS generation. The concurrent blockade of NFκB (a cellular defense mechanism) in the presence of oxidative stress is a positive attribute and this dual activity probably accounts for its ability to overcome redundant survival pathways.

It is of note that we have recently shown that siJNK-2 in prostate cancer cell lines only partially blocks the anti-cancer efficacy of DMAPT38. The anti-cancer activity in the absence of JNK-2 is probably due to other effects of oxidative stress and/or the inhibition of NFκB. This includes free oxygen radical formation leading to DNA damage by breaking phosphodiester bonds of DNA helix which in turn activates ATM (ataxia telangiectasia mutated) (and ATR (ATM-and Rad3 related) and the signal transduction pathways which

inhibit cell cycle progression10, 39. Furthermore, NFκB's control of a number of genes results in its inhibition blocking many of the hallmarks of cancer including: invasion; propagation through the cell cycle; and evasion of apoptosis40-46. Ongoing work using IκB super-repressor will determine the relative contribution of NFκB inhibition to DMAPT's mechanism of action.

DMAPT's effects are probably also dependent upon the pathways activated in each unique cancer cell. To exemplify this fact, DMAPT caused cell cycle arrest in all cell types but the type of arrest is cell type dependent - brief G2 arrest in A549 – [wt, p53; wt Rb, 20, 21] and prolonged S phase arrest in UMUC-3 – [mutant p53, wt Rb28]. The effects are independent of p53 and Rb status. Interestingly, DMAPT retained cell cycle inhibitory effects despite the presence of a tobacco carcinogen and displayed cell type-dependent effects on cell cycle regulatory proteins. DMAPT suppressed cyclin D1 expression in BEAS2B but not in RT4, UMUC-3 and A549. The lack of inhibition of cyclin D1 expression with DMAPT treatment despite NFκB inhibition in these cell types could be due to the redundancy of transcription factors such as AP-1, STATs and CREB:CREM:ATF-2, which regulate cyclin D1 expression47. Induction of p21 was observed in all the cell lines we have examined so far. Similarly, TAp73 was induced in UMUC-3 and A549. The data presented suggests that TAp73 has a limited (if any) role in DMAPT-mediated induction of p21.

In summary, DMAPT is active as a single agent in two smoking related tumors in both *in vitro* and *in vivo* models and in both early and late stage cancers. Work to date has also shown it has the positive attribute of concurrently generating oxidative stress and blocking the transcription factor NFκB. However, further work is required to determine the relevant contribution of each observation to DMAPT's mechanism of action. In addition, the data in this paper supports the conduct of clinical trials in bladder and non small lung cancers upon successful completion of the ongoing phase 1 clinical trial.

## Supplementary Material

Refer to Web version on PubMed Central for supplementary material.

## Acknowledgments

We would like to acknowledge Dr Craig Jordan, PhD (University of Rochester) for his suggestions and constructive review of the manuscript.

This work was supported in part by grants from donations from Gerry Gillette and Family, Walther Cancer Institute (CS), FAMRI Clinical Investigator Award # 052319 and NIH R03 CA137796 (HN), Kentucky Foundation (PC)

## REFERENCES

1. Jemal A, Siegel R, Ward E, Hao Y, Xu J, Murray T, Thun MJ. Cancer statistics, 2008. CA Cancer J Clin. 2008; 58:71–96. [PubMed: 18287387]
2. Sedjo RL, Byers T, Barrera E Jr. Cohen C, Fontham ET, Newman LA, Runowicz CD, Thorson AG, Thun MJ, Ward E, Wender RC, Eyre HJ. A midpoint assessment of the American Cancer Society challenge goal to decrease cancer incidence by 25% between 1992 and 2015. CA Cancer J Clin. 2007; 57:326–40. [PubMed: 17989128]
3. Shepherd FA, Rodrigues Pereira J, Ciuleanu T, Tan EH, Hirsh V, Thongprasert S, Campos D, Maoleekoonpiroj S, Smylie M, Martins R, van Kooten M, Dediu M, et al. Erlotinib in previously treated non-small-cell lung cancer. N Engl J Med. 2005; 353:123–32. [PubMed: 16014882]
4. Sandler A, Gray R, Perry MC, Brahmer J, Schiller JH, Dowlati A, Lilenbaum R, Johnson DH. Paclitaxel-carboplatin alone or with bevacizumab for non-small-cell lung cancer. N Engl J Med. 2006; 355:2542–50. [PubMed: 17167137]

5. Bork PM, Schmitz ML, Kuhnt M, Escher C, Heinrich M. Sesquiterpene lactone containing Mexican Indian medicinal plants and pure sesquiterpene lactones as potent inhibitors of transcription factor NF-kappaB. FEBS Lett. 1997; 402:85–90. [PubMed: 9013864]

6. Wen J, You KR, Lee SY, Song CH, Kim DG. Oxidative stress-mediated apoptosis. The anticancer effect of the sesquiterpene lactone parthenolide. J Biol Chem. 2002; 277:38954–64. [PubMed: 12151389]

7. Hehner SP, Heinrich M, Bork PM, Vogt M, Ratter F, Lehmann V, Schulze-Osthoff K, Droge W, Schmitz ML. Sesquiterpene lactones specifically inhibit activation of NF-kappa B by preventing the degradation of I kappa B-alpha and I kappa B-beta. J Biol Chem. 1998; 273:1288–97. [PubMed: 9430659]

8. Sweeney C, Li L, Shanmugam R, Bhat-Nakshatri P, Jayaprakasan V, Baldridge LA, Gardner T, Smith M, Nakshatri H, Cheng L. Nuclear factor-kappaB is constitutively activated in prostate cancer in vitro and is overexpressed in prostatic intraepithelial neoplasia and adenocarcinoma of the prostate. Clin Cancer Res. 2004; 10:5501–7. [PubMed: 15328189]

9. Mendonca MS, Chin-Sinex H, Gomez-Millan J, Datzman N, Hardacre M, Comerford K, Nakshatri H, Nye M, Benjamin L, Mehta S, Patino F, Sweeney C. Parthenolide sensitizes cells to X-ray-induced cell killing through inhibition of NF-kappaB and split-dose repair. Radiat Res. 2007; 168:689–97. [PubMed: 18088190]

10. Gopal YN, Chanchorn E, Van Dyke MW. Parthenolide promotes the ubiquitination of MDM2 and activates p53 cellular functions. Mol Cancer Ther. 2009; 8:552–62. [PubMed: 19276167]

11. Curry EA 3rd, Murry DJ, Yoder C, Fife K, Armstrong V, Nakshatri H, O'Connell M, Sweeney CJ. Phase I dose escalation trial of feverfew with standardized doses of parthenolide in patients with cancer. Invest New Drugs. 2004; 22:299–305. [PubMed: 15122077]

12. Shanmugam R, Jayaprakasan V, Gokmen-Polar Y, Kelich S, Miller KD, Yip-Schneider M, Cheng L, Bhat-Nakshatri P, Sledge GW Jr. Nakshatri H, Zheng Q-H, Miller MA, et al. Restoring chemotherapy and hormone therapy sensitivity by parthenolide in a xenograft hormone refractory prostate cancer model. Prostate. 2006; 66:1498–511. [PubMed: 16921510]

13. Neelakantan S, Nasim S, Guzman ML, Jordan CT, Crooks PA. Aminoparthenolides as novel anti-leukemic agents: Discovery of the NF-kappaB inhibitor, DMAPT (LC-1). Bioorg Med Chem Lett. 2009; 19:4346–9. [PubMed: 19505822]

14. Guzman ML, Rossi RM, Neelakantan S, Li X, Corbett CA, Hassane DC, Becker MW, Bennett JM, Sullivan E, Lachowicz JL, Vaughan A, Sweeney CJ, et al. An orally bioavailable parthenolide analog selectively eradicates acute myelogenous leukemia stem and progenitor cells. Blood. 2007; 110:4427–35. [PubMed: 17804695]

15. Hewamana S, Alghazal S, Lin TT, Clement M, Jenkins C, Guzman ML, Jordan CT, Neelakantan S, Crooks PA, Burnett AK, Pratt G, Fegan C, et al. The NF-kappaB subunit Rel A is associated with in vitro survival and clinical disease progression in chronic lymphocytic leukemia and represents a promising therapeutic target. Blood. 2008; 111:4681–9. [PubMed: 18227347]

16. Jenkins C, Hewamana S, Gilkes A, Neelakantan S, Crooks P, Mills K, Pepper C, Burnett A. Nuclear factor-kappaB as a potential therapeutic target for the novel cytotoxic agent LC-1 in acute myeloid leukaemia. Br J Haematol. 2008; 143:661–71. [PubMed: 19036014]

17. Vegeler RC, Yip-Schneider MT, Ralstin M, Wu H, Crooks PA, Neelakantan S, Nakshatri H, Sweeney CJ, Schmidt CM. Effect of celecoxib and novel agent LC-1 in a hamster model of lung cancer. J Surg Res. 2007; 143:169–76. [PubMed: 17950089]

18. Yip-Schneider MT, Wu H, Njoku V, Ralstin M, Holcomb B, Crooks PA, Neelakantan S, Sweeney CJ, Schmidt CM. Effect of celecoxib and the novel anti-cancer agent, dimethylamino-parthenolide, in a developmental model of pancreatic cancer. Pancreas. 2008; 37:e45–53. [PubMed: 18815538]

19. Yip-Schneider MT, Wu H, Ralstin M, Yiannoutsos C, Crooks PA, Neelakantan S, Noble S, Nakshatri H, Sweeney CJ, Schmidt CM. Suppression of pancreatic tumor growth by combination chemotherapy with sulindac and LC-1 is associated with cyclin D1 inhibition in vivo. Mol Cancer Ther. 2007; 6:1736–44. [PubMed: 17541034]

20. Chang GC, Yu CT, Tsai CH, Tsai JR, Chen JC, Wu CC, Wu WJ, Hsu SL. An epidermal growth factor inhibitor, Gefitinib, induces apoptosis through a p53-dependent upregulation of pro-

apoptotic molecules and downregulation of anti-apoptotic molecules in human lung adenocarcinoma A549 cells. Eur J Pharmacol. 2008; 600:37–44. [PubMed: 18973751]

21. Mack PC, Gandara DR, Bowen C, Edelman MJ, Paglieroni T, Schnier JB, Gelmann EP, Gumerlock PH. RB status as a determinant of response to UCN-01 in non-small cell lung carcinoma. Clin Cancer Res. 1999; 5:2596–604. [PubMed: 10499638]
22. Sun SH, Zheng M, Ding K, Wang S, Sun Y. A small molecule that disrupts Mdm2-p53 binding activates p53, induces apoptosis and sensitizes lung cancer cells to chemotherapy. Cancer Biol Ther. 2008; 7:845–52. [PubMed: 18340116]
23. Ikediobi ON, Davies H, Bignell G, Edkins S, Stevens C, O'Meara S, Santarius T, Avis T, Barthorpe S, Brackenbury L, Buck G, Butler A, et al. Mutation analysis of 24 known cancer genes in the NCI-60 cell line set. Molecular Cancer Therapeutics. 2006; 5:2606–12. [PubMed: 17088437]
24. Lonardo F, Dragnev KH, Freemantle SJ, Ma Y, Memoli N, Sekula D, Knauth EA, Beebe JS, Dmitrovsky E. Evidence for the epidermal growth factor receptor as a target for lung cancer prevention. Clin Cancer Res. 2002; 8:54–60. [PubMed: 11801540]
25. Chang YC, Lin P. Trans, trans-2,4-decadienal induced cell proliferation via p27 pathway in human bronchial epithelial cells. Toxicol Appl Pharmacol. 2008; 228:76–83. [PubMed: 18187174]
26. Decesse JT, Medjkane S, Datto MB, Cremisi CE. RB regulates transcription of the p21/WAF1/CIP1 gene. Oncogene. 2001; 20:962–71. [PubMed: 11314031]
27. Lehman TA, Modali R, Boukamp P, Stanek J, Bennett WP, Welsh JA, Metcalf RA, Stampfer MR, Fusenig N, Rogan EM, et al. p53 mutations in human immortalized epithelial cell lines. Carcinogenesis. 1993; 14:833–9. [PubMed: 8504475]
28. Sanchez-Carbayo M, Socci ND, Charytonowicz E, Lu M, Prystowsky M, Childs G, Cordon-Cardo C. Molecular profiling of bladder cancer using cDNA microarrays: defining histogenesis and biological phenotypes. Cancer Res. 2002; 62:6973–80. [PubMed: 12460915]
29. Backhus LM, Sievers E, Lin GY, Castanos R, Bart RD, Starnes VA, Bremner RM. Perioperative cyclooxygenase 2 inhibition to reduce tumor cell adhesion and metastatic potential of circulating tumor cells in non-small cell lung cancer. J Thorac Cardiovasc Surg. 2006; 132:297–303. [PubMed: 16872953]
30. Pugh TD, King JH, Koen H, Nychka D, Chover J, Wahba G, He YH, Goldfarb S. Reliable stereological method for estimating the number of microscopic hepatocellular foci from their transections. Cancer Res. 1983; 43:1261–8. [PubMed: 6825098]
31. Zhang S, Ong C-N, Shen H-M. Critical roles of intracellular thiols and calcium in parthenolide-induced apoptosis in human colorectal cancer cells. Cancer Letters. 2004; 208:143–53. [PubMed: 15142672]
32. Temkin V, Karin M. From death receptor to reactive oxygen species and c-Jun N-terminal protein kinase: the receptor-interacting protein 1 odyssey. Immunol Rev. 2007; 220:8–21. [PubMed: 17979836]
33. Nakshatri H, Rice SE, Bhat-Nakshatri P. Antitumor agent parthenolide reverses resistance of breast cancer cells to tumor necrosis factor-related apoptosis-inducing ligand through sustained activation of c-Jun N-terminal kinase. Oncogene. 2004; 23:7330–44. [PubMed: 15286701]
34. Anand P, Thomas SG, Kunnumakkara AB, Sundaram C, Harikumar KB, Sung B, Tharakan ST, Misra K, Priyadarsini IK, Rajasekharan KN, Aggarwal BB. Biological activities of curcumin and its analogues (Congeners) made by man and Mother Nature. Biochem Pharmacol. 2008; 76:1590–611. [PubMed: 18775680]
35. Slamon DJ, Leyland-Jones B, Shak S, Fuchs H, Paton V, Bajamonde A, Fleming T, Eiermann W, Wolter J, Pegram M, Baselga J, Norton L. Use of chemotherapy plus a monoclonal antibody against HER2 for metastatic breast cancer that overexpresses HER2. N Engl J Med. 2001; 344:783–92. [PubMed: 11248153]
36. Liu J, Lin A. Role of JNK activation in apoptosis: A double-edged sword. Cell Res. 2005; 15:36–42. [PubMed: 15686625]
37. Faruqi RM, Poptic EJ, Faruqi TR, De La Motte C, DiCorleto PE. Distinct mechanisms for N-acetylcysteine inhibition of cytokine-induced E-selectin and VCAM-1 expression. Am J Physiol. 1997; 273:H817–26. [PubMed: 9277499]

38. Shanmugam R, Kusumanchi K, Cheng L, Crooks P, Neelakantan S, Matthews W, Nakshatri H, Sweeney CJ. A water soluble parthenolide analogue suppresses in vivo prostate cancer growth by targeting NF-κB and generating reactive oxygen species. Prostate. 2010 (in press).
39. Kastan MB, Bartek J. Cell-cycle checkpoints and cancer. Nature. 2004; 432:316–23. [PubMed: 15549093]
40. Helbig G, Christopherson KW 2nd, Bhat-Nakshatri P, Kumar S, Kishimoto H, Miller KD, Broxmeyer HE, Nakshatri H. NF-kappaB promotes breast cancer cell migration and metastasis by inducing the expression of the chemokine receptor CXCR4. J Biol Chem. 2003; 278:21631–8. [PubMed: 12690099]
41. Jones PL, Ping D, Boss JM. Tumor necrosis factor alpha and interleukin-1beta regulate the murine manganese superoxide dismutase gene through a complex intronic enhancer involving C/EBP-beta and NF-kappaB. Mol Cell Biol. 1997; 17:6970–81. [PubMed: 9372929]
42. Zong WX, Edelstein LC, Chen C, Bash J, Gelinas C. The prosurvival Bcl-2 homolog Bfl-1/A1 is a direct transcriptional target of NF-kappaB that blocks TNFalpha-induced apoptosis. Genes Dev. 1999; 13:382–7. [PubMed: 10049353]
43. Lee HH, Dadgostar H, Cheng Q, Shu J, Cheng G. NF-kappaB-mediated upregulation of Bcl-x and Bfl-1/A1 is required for CD40 survival signaling in B lymphocytes. Proc Natl Acad Sci U S A. 1999; 96:9136–41. [PubMed: 10430908]
44. Baldini N. Multidrug resistance--a multiplex phenomenon. Nat Med. 1997; 3:378–80. [PubMed: 9095165]
45. Wang CY, Mayo MW, Baldwin AS Jr. TNF- and cancer therapy-induced apoptosis: potentiation by inhibition of NF-kappaB. Science. 1996; 274:784–7. [PubMed: 8864119]
46. Karashima T, Sweeney P, Kamat A, Huang S, Kim SJ, Bar-Eli M, McConkey DJ, Dinney CP. Nuclear factor-kappaB mediates angiogenesis and metastasis of human bladder cancer through the regulation of interleukin-8. Clin Cancer Res. 2003; 9:2786–97. [PubMed: 12855659]
47. Joyce D, Albanese C, Steer J, Fu M, Bouzahzah B, Pestell RG. NF-kappaB and cell-cycle regulation: the cyclin connection. Cytokine Growth Factor Rev. 2001; 12:73–90. [PubMed: 11312120]

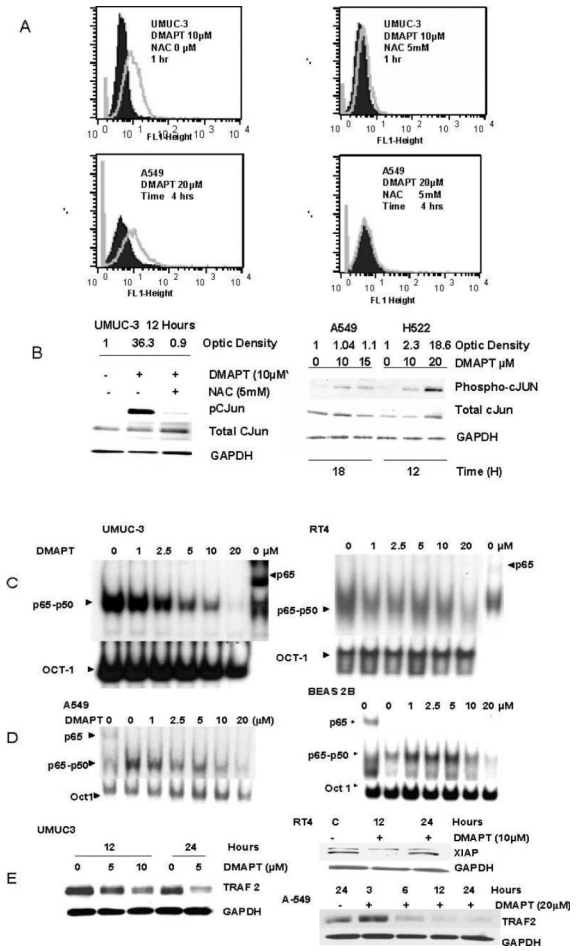


**Figure 1. DMAPT generates reactive oxygen species (ROS) and inhibits Nuclear factor kappa B in both lung and urothelial cell lines**

(A) Flow cytometric analysis using 2, 7-dichlorohydrofluorescein diacetate ($H_2$DCFDA dye) detailed the ability of DMAPT to generate ROS, which was blocked by N-acetyl cysteine (NAC) in UMUC-3 cell (upper panel) and A549 cells in (lower panel). The solid peaks are a control representing baseline ROS levels and grey peaks represent amount of ROS after exposure to drug treatment. (B) Western blotting demonstrated DMAPT treatment resulted in phosphorylation of c-Jun in both TCC (UMUC-3) and NSCLC (A549 and H522) cell lines. As observed in the left hand panel, this was substantially suppressed by pre-treatment with NAC in the UMUC-3 cell line. In the right hand panel it is noted the phosphorylation of cJUN was dose dependent in H522. (C and D) Electrophoretic mobility gel shift assays (EMSA) demonstrated constitutive NFκB DNA binding in all of the cell lines with the p65-p50 label indicating the location of this heterodimer. The presence of the most active NFκB subunit, p65, in the DNA-protein complex of both NSCLC and TCC cell lines was confirmed by a supershift with a p65 antibody. This is delineated in the last column of UMUC-3 and RT4 and the first column of A549 and BEAS2B EMSA figures. When the NFκB dimer complexes from the no DMAPT columns are compared, the location of the p65 dimer in the heterodimer complexes can be discerned. DMAPT's ability to inhibit NFκB DNA binding after 3 hours of treatment in UMUC-3 and RT4 (C) and A549 and BEAS2B (D) cell lines is shown to be dose dependent. (E) Western blotting revealed DMAPTs ability to decrease NFκB dependent proteins: TRAF-2 in UMUC-3 (left panel) as well as XIAP in RT4 and TRAF2 in A549 cells (right panel).

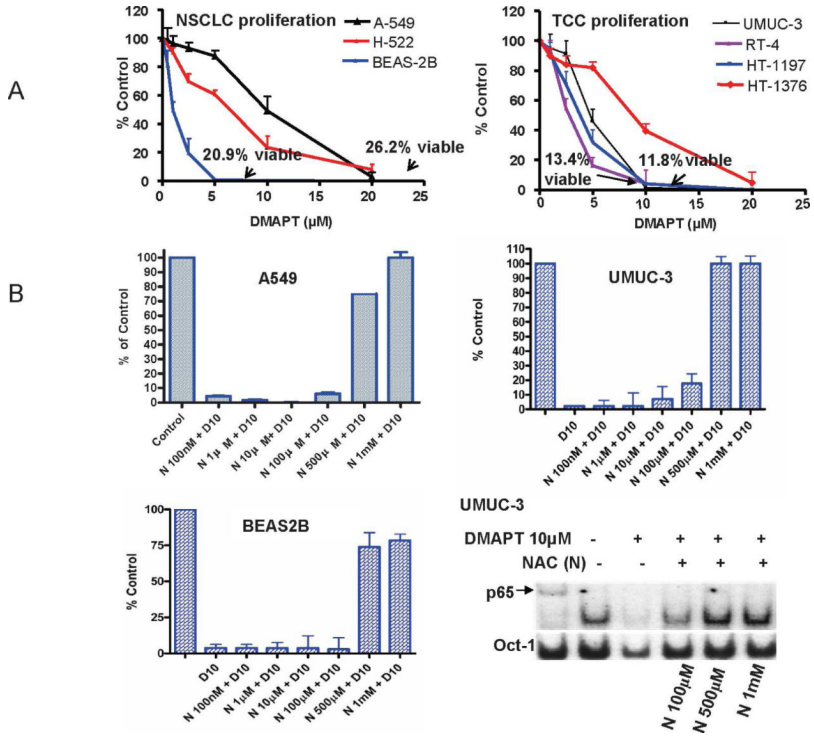


**Figure 2. DMAPT inhibits cellular proliferation of early and late neoplastic lung and urothelial cell lines**

(A) BrdU incorporation assay demonstrated DMAPT's ability to inhibit the *in vitro* proliferation of NSCLC cell lines – A549, H-222 and BEAS (left panel) and TCC cell lines - UMUC, HT1197, HT1376 and RT-4 (right panel). For each cell line 2,000 cells were placed in 100μL, drug added at concentrations of 1, 2, 5, 10 and 20 μM after 24 hours of cell growth and the percentage of cells relative to untreated control was determined after 48 hours of drug exposure. The trypan blue assay showed that after one DMAPT dose the viability for each cell line at 48 hours was 26.2% for A549 with 20 M, 20.9% for BEAS2B with 5 M; 11.8% for UMUC-3 with 10μM and 13.4% for RT4 with 10uM. (B) Using a BrdU incorporation assay NAC was observed to decrease DMAPT's *in vitro* anti-proliferative activity in UMUC-3, A549 and BEAS2B in a dose dependent manner. In all cell lines, 10 M DMAPT suppressed proliferation by greater than 90% and this was almost completely abrogated by 1mM NAC in UMUC-3 and A549 and DMAPT's anti-proliferative efficacy was limited to only 25% in BEAS2B cell line. (B, bottom right panel). Electrophoretic mobility gel shift assay demonstrating NAC abrogating DMAPT's ability to inhibit NFκB DNA binding in a dose dependent manner in UMUC-3.

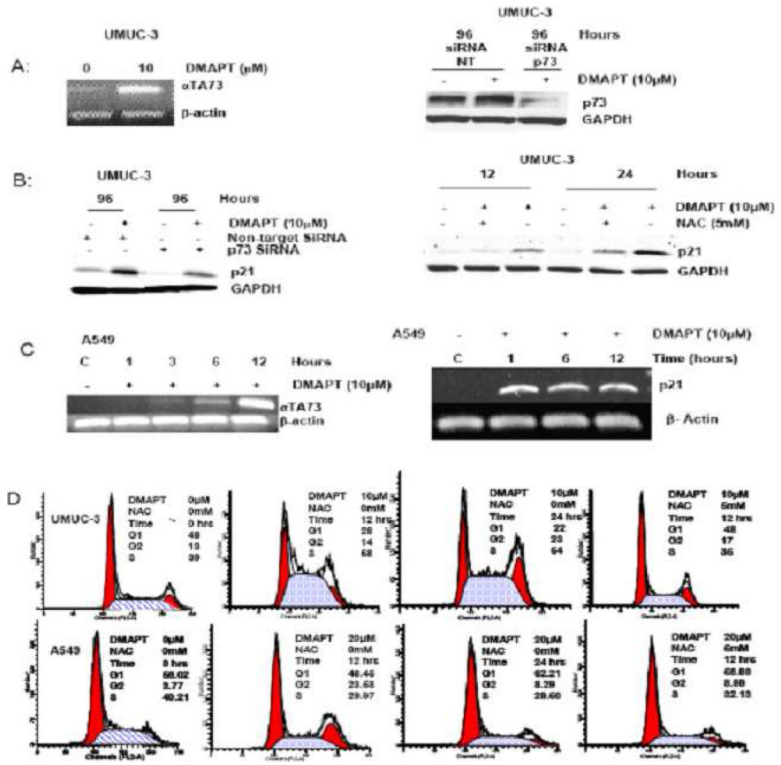


**Figure 3. DMAPT upregulates p73 and p21 and alters cell cycle distribution in a cell dependent manner**

(A) RT-PCR demonstrated DMAPT mediated upregulation of p73 in UMUC-3 (left panel) and small interference (si) RNA inhibition of p73 transcription was demonstrated by Western blot of UMUC-3 cell line with a non-target control and with and without DMAPT (right panel). (B) Western blotting demonstrated DMAPT upregulated p21 in UMUC-3 with non-target siRNA, and showed that this was partially blunted in the siRNA-p73 cell line variant (left panel). Western blotting also showed that NAC partially blocked DMAPT mediated upregulation of p21(right panel). (C) RT-PCR detailed DMAPT's ability to increase p73 (left panel) and p21 in NSCLC cell line, A549 (right panel). (D) Flow cytometric analysis demonstrated DMAPT induced accumulation of cells in S phase at 12 and 24 hours in UMUC-3 (top panel) and G2 phase at 12 hours but not 24 hours in A549 cells (bottom panel) . NAC blocked cell cycle effects of DMAPT in both cell lines.

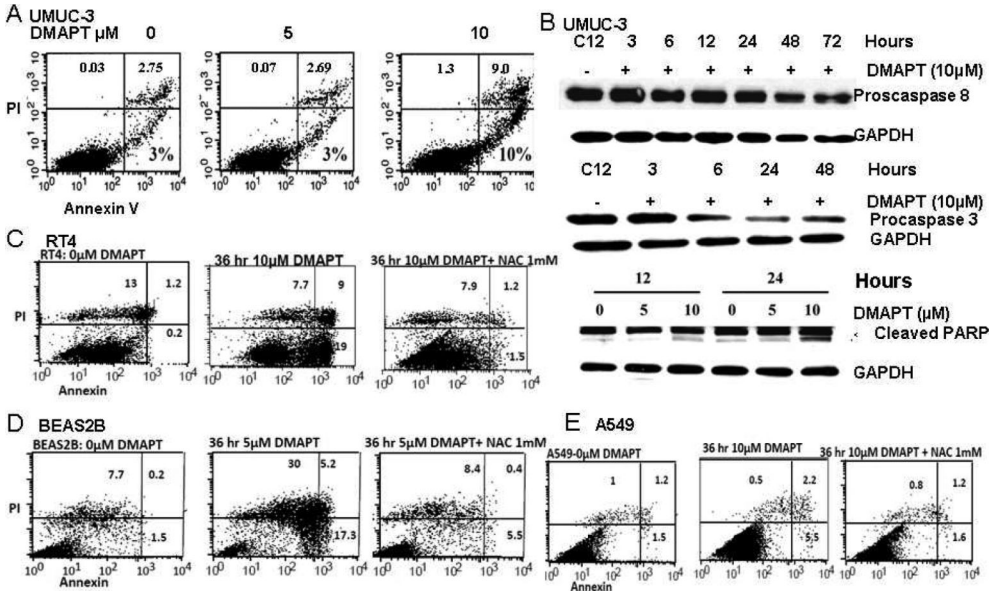


**Figure 4. DMAPT induces cell death in a cell dependent manner**

(A) Flow cytometry with propidium iodine and Annexin V staining showed the ability of DMAPT to induce early and late apoptosis in UMUC-3 with 5 and 10 M. In this assay, the upper left quadrant with predominant PI staining represents necrosis, the upper right, combined PI and annexin staining represents late/atypical apoptosis and bottom right with predominant annexin staining represents early/typical apoptosis. (B) Western blotting of proteins in UMUC-3 detailed DMAPT induced cleavage of procaspase 8, procaspase 3, and PARP. Flow cytometry demonstrated DMAPT induced early and late apoptosis in RT4 (C), BEAS-2B (D) and A549 (E). In BEAS-2B, DMAPT also induced substantial necrosis. All of these types of cell death were blocked by NAC in RT4, BEAS2B and A549.

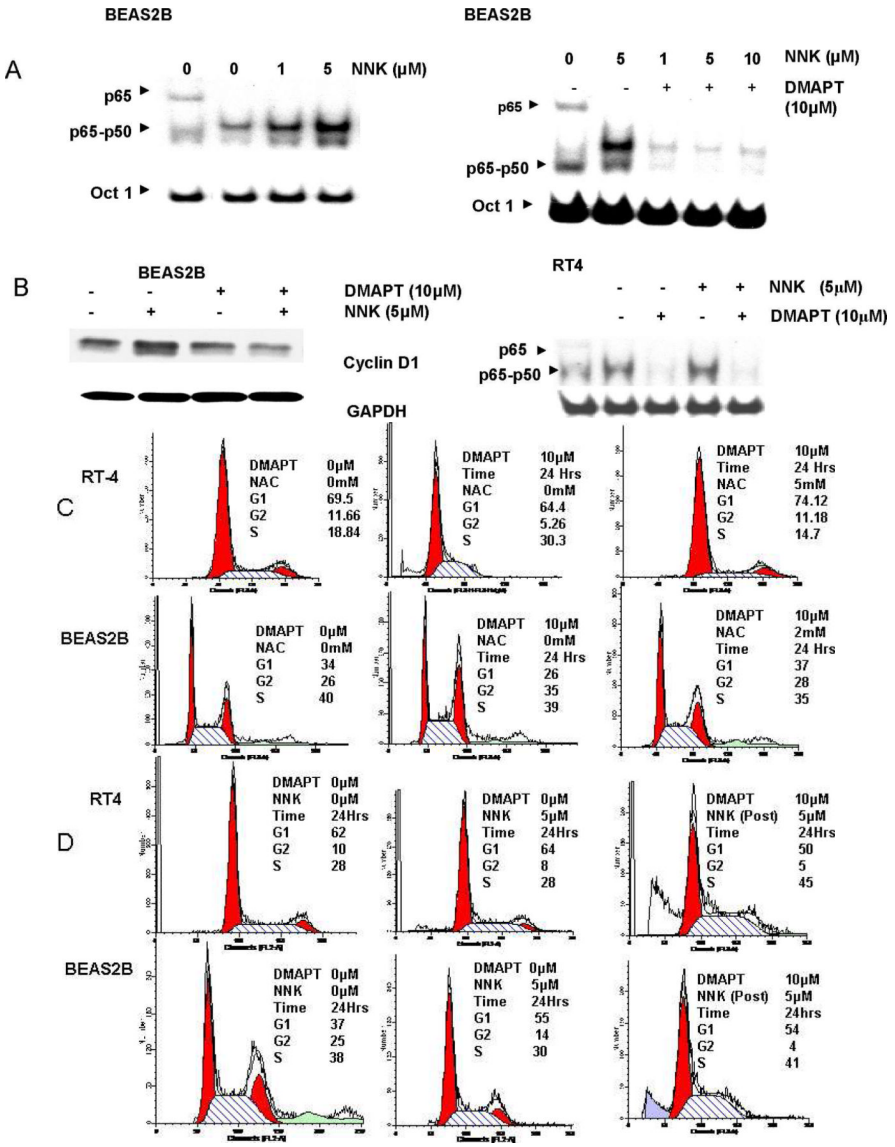


**Figure 5. DMAPT inhibits NFκB and cancer cell cycle progression despite presence of tobacco associated carcinogen, NNK, in early smoking related cancers**

(A) EMSA detailed NNK increased NFκB DNA binding in a dose dependent manner in BEAS2B (left panel) and that DMAPT was able to block NNK-induced NFκB DNA binding in BEAS2B (right panel). (B) Western blotting detailed NNK increased the levels of cyclin D1 protein and that this was blocked by DMAPT (left panel). EMSA revealed NNK did not increase NFκB DNA binding in RT4 nor did it block the ability of DMAPT to inhibit NFκB DNA binding (right panel). In all EMSA figures the first panel is p65 supershift demonstrating location of p65 in the p65-50 heterodimer in the other lanes. (C) Flow cytometry demonstrated DMAPT induced S phase and G2 phase accumulation in RT4 and BEAS2B, respectively. These changes were present at 12 and 24 hours in both cell lines (data not shown for 12 hour time point) and were blocked by NAC. (D) NNK did not alter cell cycle distribution in RT4 but did increase the number of BEAS2B cells in G1 phase at 24 hours (37% in control versus 55% with NNK treatment). The ability of DMAPT to induce S phase accumulation in RT4 was not abrogated by exposing the cells to NNK after DMAPT (top panel). In BEAS2B, whereas DMAPT alone induced G2 phase accumulation

(C, lower panel), DMAPT treatment followed by NNK exposure caused cells to accumulate in G1 and S phases.

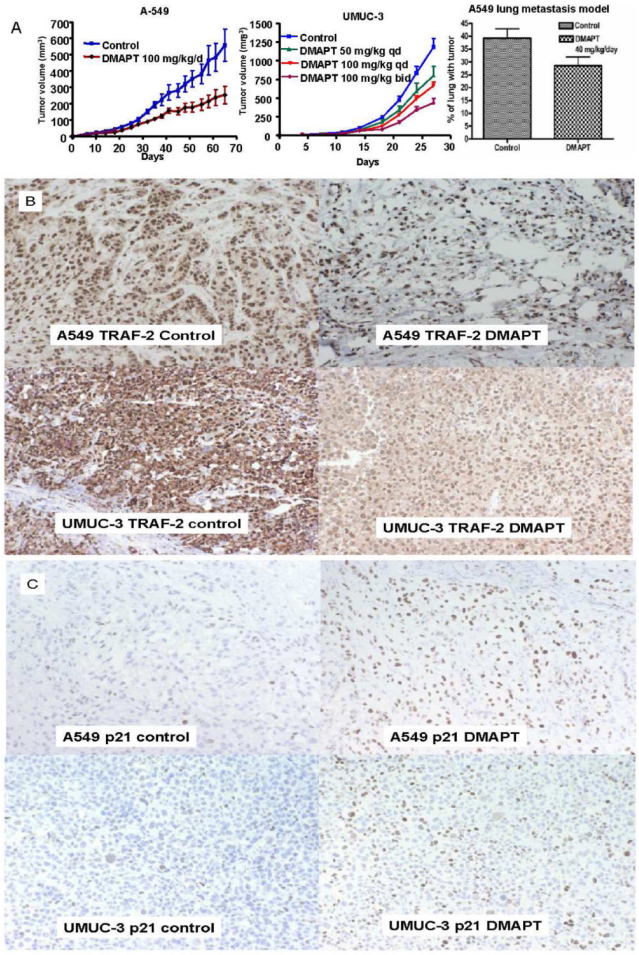


**Figure 6. DMAPT has *in vivo* anti-cancer activity in both transitional cell and non-small lung cancers**

(A) Established xenograft experiments with A549 (left panel) and UMUC-3 (middle panel) cells were conducted with the cell lines injected into the subcutaneous tissue of the flanks of athymic male nude mice. Treatment was commenced when tumors were palpable at day 7. DMAPT was given by daily oral gavage and was able to suppress tumor growth relative to untreated control in A549. In UMUC-3, DMAPT's ability to suppress tumor growth was observed to be dose dependent with 100 mg/kg twice per day (bid) being more effective than 50 mg/kg or 100 mg/kg daily (qd). The ability of orally administered DMAPT to inhibit the *in vivo* metastatic process (implantation of circulating cells) of A549 cell lines (right panel) was demonstrated by measuring the relative volume of lung involved with cancer 60 days after cells were injected by tail vein. Treatment was commenced on day 1 with daily oral DMAPT given by oral gavage for 48 days. (B) TRAF-2 immunohistochemical staining of tumors is depicted by the brown staining of cells. The tumors were extracted from the control and DMAPT single agent arms at the time of sacrifice of both A549 and UMUC-3 experiments. The photographs of the microscopic images demonstrate that compared with control, DMAPT decreased the expression of TRAF-2 in both A549 (top panel) and UMUC-3 (bottom panel) as evidenced by decreased intensity of brown staining of cytoplasm in both cell lines as well as in the nuclei of UMUC-3 cells. (C) p21 immunohistochemical staining of tumors is depicted by brown staining of cells. The tumors were extracted from the control and DMAPT single agent arms at the time of sacrifice of both A549 and UMUC-3 experiments. The photographs of the microscopic images

demonstrate that compared with control, DMAPT increased the expression of p21 in both A549 (top panel) and UMUC-3 (bottom panel) as evidenced by increased amount of brown staining of the nuclei.